

Magnetic Properties of NbSi_2N_4 , VSi_2N_4 , and VSi_2P_4 Monolayers

Md. Rakibul Karim Akanda^{a)} and Roger K. Lake^{b)}

Laboratory for Terahertz and Terascale Electronics (LATTE), Department of Electrical and Computer Engineering, University of California, Riverside, CA 92521, USA

The recent demonstration of MoSi_2N_4 and its exceptional stability to air, water, acid, and heat has generated intense interest in this family of two-dimensional (2D) materials. Among these materials, monolayers of NbSi_2N_4 , VSi_2N_4 , and VSi_2P_4 are semiconducting, easy-plane ferromagnets with negligible in-plane magnetic anisotropy. They thus satisfy a necessary condition for exhibiting a dissipationless spin superfluid mode. The Curie temperatures of monolayer VSi_2P_4 and VSi_2N_4 are determined to be above room temperature based on Monte Carlo and density functional theory calculations. The magnetic moments of VSi_2N_4 can be switched from in-plane to out-of-plane by applying tensile biaxial strain or electron doping.

Two dimensional (2D) layered materials with transition metals have been of interest for many decades due to the correlated phenomena and multiple polymorphs and phases that they can exhibit such as charge density waves,¹ superconductivity,² and magnetism.³ The ability to exfoliate or grow single monolayers renewed the interest in these materials for possible electronic and optoelectronic applications^{4,5} by both traditional transistor type devices^{6,7} and by exploiting external control of their phase transitions.⁸ The relatively recent demonstration of magnetism in single monolayer of CrI_3 ⁹ and bilayers of $\text{Cr}_2\text{Ge}_2\text{Te}_6$ ¹⁰ has spurred intense experimental and theoretical activity to find other 2D magnetic materials with higher transition temperatures.^{11–18}

The most recent addition to the family of 2D materials are the transition metal silicon nitrides, phosphides, and arsenides with the chemical formulas MA_2Z_4 , where M is the transition metal, $A \in \{\text{Si}, \text{Ge}\}$, and $Z \in \{\text{N}, \text{P}, \text{As}\}$.¹⁹ High quality multilayers and monolayers of MoSi_2N_4 were grown using chemical vapor deposition, and what was particularly notable was their stability to air, water, acid, and heat that was unprecedented among transition metal 2D materials.¹⁹ This rather mundane property is highly desirable for manufacturing applications. While BN encapsulation is an effective solution for stabilizing reactive 2D materials for laboratory experiments,²⁰ it is less than ideal for manufacturing. Only MoSi_2N_4 was experimentally characterized in detail, WSi_2N_4 was also grown, and 12 materials were simulated with density functional theory (DFT) and found to be stable. Among these 12, two of the nitrides, VSi_2N_4 and NbSi_2N_4 , were identified as magnetic.

This work motivated immediate follow-on theoretical investigations of this material family both determining properties of the materials and extending the list of stable materials.^{21–29} The most extensive theoretical survey found 32 thermodynamically and dynamically stable compounds of the form MA_2Z_4 .²⁴ Of these, 6 were magnetic: VSi_2N_4 , VSi_2P_4 , NbSi_2N_4 , VGe_2N_4 , VGe_2P_4 , and TaGe_2N_4 . Based on the formation enthalpies, a Si based

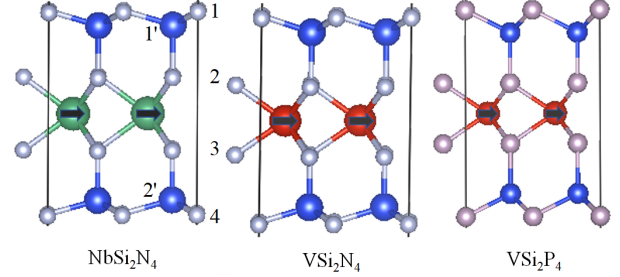


FIG. 1. Structures and magnetic orientations of α_1 - NbSi_2N_4 , α_1 - VSi_2N_4 , and α_1 - VSi_2P_4 . Blue atoms are Si, white atoms are N, and pink atoms are P. The directions of the magnetic moments are shown on the transition metals Nb and V. All materials are easy-plane, semiconducting ferromagnets.

compound MSi_2Z_4 is approximately 3 times more stable than its equivalent Ge based compound MGe_2Z_4 , and a silicon nitride compound MSi_2N_4 is also approximately 3 times more stable than its equivalent silicon phosphide compound MSi_2P_4 .

Other recent works investigated MSi_2Z_4 bilayers ($M = \text{Ti}, \text{Cr}, \text{Mo}$; $Z = \text{N}, \text{P}$) for their sensitivity to vertical strain^{27,28}, and MoSi_2N_4 and WSi_2N_4 for their sensitivity to biaxial strain and vertical applied electric field.²⁷ It was found that vertical strain can cause an insulator to metal transition;²⁸ biaxial strain can lead to an indirect to direct bandgap transition;²⁷ and that an applied electric field can result in an insulator to metal transition.²⁷ A theoretical investigation of 2D-2D contacts to monolayer MoSi_2N_4 using NbS_2 and graphene found ultralow p-type Schottky barriers with NbS_2 contacts and approximately equal n-type and p-type Schottky barriers with graphene contacts.²² The graphene Schottky barriers were shown to be tunable with an applied vertical electric field.

In this letter, we theoretically investigate the magnetic properties of the three Si based magnetic materials: VSi_2N_4 , VSi_2P_4 , NbSi_2N_4 . Values of the exchange constants and magnetic anisotropy energies are determined, and the Curie temperatures are calculated. The Curie temperatures of VSi_2N_4 and VSi_2P_4 are near or at room temperature and above, depending on the model used, whereas the Curie temperature of NbSi_2N_4 is low. Therefore, the primarily focus will be on the two vanadium

^{a)} makan001@ucr.edu

^{b)} Corresponding author: rlake@ece.ucr.edu

compounds. The magnetic anisotropy energies of VSi_2N_4 and VSi_2P_4 are calculated as a function of uniaxial and biaxial strain and electron and hole doping.

These materials can exist in a variety of hexagonal phases. Ref. [24] calculated the formation energies of 30 different phases and found that the lowest energy phase of NbSi_2N_4 and VSi_2N_4 was the α_1 phase, which is the same phase as the lowest energy phase of MoSi_2N_4 . The formation energy of the next higher energy phase (δ_4) of NbSi_2N_4 was 13 meV per atom higher than the α_1 phase, and the formation energy of the next higher energy phase (β_2) of VSi_2N_4 was 6 meV per atom higher than the α_1 phase. For VSi_2P_4 , the lowest energy phase was δ_4 with a formation energy 0.3 meV below that of α_1 . Since the formation energy of the α_1 phase of VSi_2P_4 is so close to that of the δ_4 phase, and since the δ_4 phase has been previously analyzed²⁴, we will consider the α_1 phase of all 3 materials: NbSi_2N_4 , VSi_2N_4 , and VSi_2P_4 . We note that the piezoelectric and magnetic properties of the α_1 phase of VSi_2P_4 have recently been investigated with DFT using the generalized gradient approximation (GGA).²¹

DFT combined with Monte Carlo (MC) calculations are applied to determine the electronic and magnetic properties of these materials. The magnetic anisotropy energy (MAE) and exchange energy are evaluated from DFT calculations implemented in the Vienna ab initio simulation package (VASP).³⁰ The electron-core interactions are described by the projected augmented wave (PAW) potentials.³¹ Electronic structure is calculated using three different functionals: GGA as parameterized by Perdew-Burke-Ernzerhof (PBE), PBE plus the Hubbard U correction (PBE+U), and the Heyd-Scuseria-Ernzerhof hybrid functional (HSE06).^{32–35} The PBE+U calculation includes a Hubbard U correction term $U_{\text{eff}} = 1$ eV for the V atom where $U_{\text{eff}} = U - J$.^{36,37} For calculations of the MAE, spin orbit coupling (SOC) must also be included. All plots shown for the MAE are the results from PBE(SOC)+U calculations. The cutoff energies for expanding the plane wave basis are 600 eV. Integration over the Brillouin zone uses a Monkhorst–Pack scheme with a Γ -centered $16 \times 16 \times 1$ k-point grid, an energy broadening parameter of 50 meV, and the total energy is converged to 10^{-6} eV. Structures are relaxed until the forces are less than 0.001 eV/Å. A vacuum spacing of 20 Å is used in the direction normal to the 2D monolayer to eliminate the interactions from periodic images. The calculated lattice constants for NbSi_2N_4 , VSi_2N_4 , and VSi_2P_4 are 2.96 Å, 2.88 Å, and 3.47 Å, respectively, and they are very close to previous reported results.^{19,21}

Uniaxial strain is applied along the x axis corresponding to lattice vector a_1 . The applied strain is evaluated using $\epsilon = (a - a_0)/a_0 \times 100\%$, where a and a_0 are the lattice parameters of the strained and unstrained monolayer. Biaxial strain is applied by uniformly varying both in-plane lattice constants. For each strain, the atomic positions are relaxed using the DFT parameters described above. Spin-polarized self consistent calculations are per-

formed with the relaxed structure for each strain to obtain the charge density. Using the charge densities, total energies are calculated in the presence of spin orbit coupling (SOC) for in-plane (E_{\parallel}) and out-of-plane (E_{\perp}) magnetization to find the magnetic anisotropy energy (MAE). The MAE is defined as $E_{\text{MAE}} = E_{\perp} - E_{\parallel}$. Positive magnetic anisotropy indicates that in-plane magnetization is favored. The values provided in meV are per magnetic atom, which for these 3 materials under consideration, are also per unit cell.

To investigate the transition temperatures, a nearest neighbor Heisenberg type Hamiltonian with magnetic anisotropy and long range dipole-dipole interactions is constructed,

$$H = -\frac{1}{2}J \sum_{\langle i,j \rangle} \mathbf{S}_i \cdot \mathbf{S}_j + k_u \sum_i (S_i^z)^2 + H_{dd}, \quad (1)$$

where \mathbf{S}_i is the spin for magnetic atom i , $\langle i, j \rangle$ are the indices of nearest neighbor magnetic atoms, $k_u > 0$ is the easy-plane magnetic anisotropy energy per magnetic atom, and H_{dd} is the dipole-dipole interaction. The exchange energies (J) of these materials are calculated from the total energy differences between the antiferromagnetic (E_{AFM}) and ferromagnetic (E_{FM}) states.^{38–41} With six nearest neighbours in the monolayer of 2D hexagonal lattice, the nearest-neighbor exchange energy is given by,^{40–42} $J = (E_{\text{AFM}} - E_{\text{FM}})/12$. In these monolayer materials all of the magnetic atoms are in the same plane. The second neighbor exchange energies were previously determined for VSi_2P_4 and found to be negligible compared to the nearest neighbor energies,²⁴ and, therefore, they are ignored. The Curie temperatures are determined from Monte Carlo (MC) calculations as implemented in the VAMPIRE software package using a 10×10 supercell.^{43,44} The MC calculations incorporate the magnetic anisotropy energies, the magnetic moments, the exchange energies, lattice constants, and atomic positions determined from the DFT calculations, and they also include the long range dipolar interactions. This MC approach has been used to determine the Curie temperatures in other monolayer 2D materials such as VSi_2P_4 , VI_3 , CrSBr , and CrSeBr .^{24,45,46} We note that the Curie temperatures in other monolayer 2D materials determined from the MC approach have been shown to compare well to temperatures determined from renormalized spin wave theory (RSWT). For example, the MC/RSWT predicted Curie temperatures for monolayer CrSBr and CrSeBr were 168/150 K and 150/152 K, respectively.⁴⁶

The structures and the ground state orientations of the magnetic moments of NbSi_2N_4 , VSi_2N_4 , and VSi_2P_4 are shown in Fig. 1, and the spin-resolved band structure for VSi_2N_4 and VSi_2P_4 , calculated with the HSE06 and PBE+U functionals, are shown in Fig. 2. The band structure for all three materials calculated with PBE, PBE+U, and HSE06 are shown in the Fig. S3 of the Supplement, and the d-orbital resolved bands of VSi_2N_4 and VSi_2P_4 are shown in Fig. S2. For all 3 materials at Γ , the two isolated narrow bands near the Fermi level

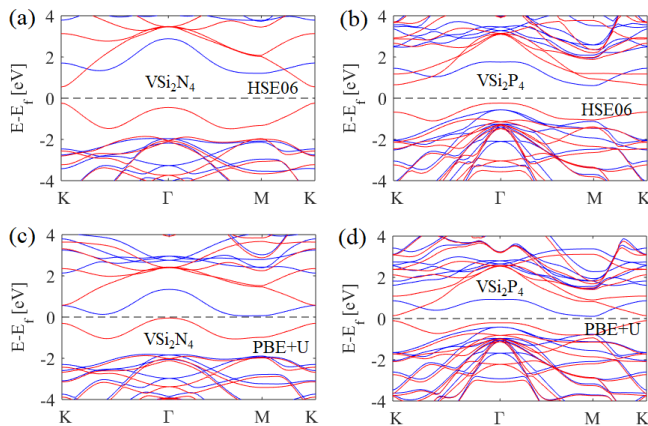


FIG. 2. Spin resolved energy bands of VSi_2N_4 and VSi_2P_4 calculated with (a,b) HSE06 and (c,d) PBE+U. Spin up bands are red and spin down bands are blue. The two spin-split, narrow bands on either side of the Fermi level are d-orbital bands centered on the transition metal.

are spin-polarized, d_{z^2} – orbital bands centered on the transition metal atoms. Near K, these bands transition to $d_{x^2-y^2}$. The next higher conduction band is primarily $d_{x^2-y^2}$ at Γ , and it transitions to d_{z^2} at K. The electronic structures from the HSE06 calculations show the following properties. In VSi_2N_4 and VSi_2P_4 , the higher spin-up conduction band at Γ crosses the lower spin-down band near K where the orbital composition of the two bands switch, $d_{z^2} \iff d_{x^2-y^2}$. VSi_2N_4 is direct gap (0.78 eV) at K with a $d_{x^2-y^2}$ spin-up valence band and a d_{z^2} spin-up conduction band. VSi_2P_4 is indirect gap (0.84 eV) with the d_{z^2} spin-up valence band edge at Γ and a mixed $d_{z^2} + d_{x^2-y^2}$ spin-down conduction band edge at M (the spin-up band at K is 40 meV higher). NbSi_2N_4 is indirect gap (0.54 eV) with the spin-up d_{z^2} valence band at Γ and a mixed orbital $d_{z^2} + d_{x^2-y^2}$ spin-down conduction band near M. The lower valence bands are primarily p-orbital bands which come from the N and P atoms. At the PBE level of theory, all 3 materials are semi-metals. Adding the Hubbard U correction creates a small gap at the Fermi level for VSi_2N_4 and VSi_2P_4 . Adding a percentage of exact exchange with the HSE06 functional increases the gap substantially. We note that the HSE06 calculations match those reported in the Supplement of Ref. [24].

The equilibrium NbSi_2N_4 , VSi_2N_4 , and VSi_2P_4 monolayers are easy-plane, semi-conducting ferromagnets. The calculated equilibrium magnetic moments, exchange energies, magnetic anisotropy energies, and Curie temperatures are shown in Table I for different levels of theory. The magnetic moments are comparable to those from prior studies.^{19,21} The positive MAE values indicate in-plane alignment of the magnetic moments. Within the energy resolution of our calculations (1 μeV), the total energy is independent of the angle of the magnetic moment within the plane of the monolayer. Since the monolayers are insulating, easy-plane FMs with ex-

Materials (Theory)	Magnetic Moment (μ_B)	Exchange energy ($\times 10^{-21}$ J)	MAE ($\frac{\text{MJ}}{\text{m}^3}$)	T_C (K)
NbSi_2N_4 (PBE)	0.32	0.064	0.30	12
VSi_2N_4 (PBE)	0.93	1.50	0.24	301
VSi_2P_4 (PBE)	0.96	1.11	0.14	235
VSi_2N_4 (PBE+U)	1.05	2.53	0.25	452
VSi_2P_4 (PBE+U)	1.04	1.77	0.11	350
VSi_2N_4 (HSE06)	1.19	2.80	--	*506

TABLE I. Magnetic moment, exchange energy per link, equilibrium magnetic anisotropy energy (MAE), and Curie temperature, calculated using different functionals for NbSi_2N_4 , VSi_2N_4 , and VSi_2P_4 . * T_C is calculated using the HSE06 exchange energy and the PBE(SOC)+U MAE.

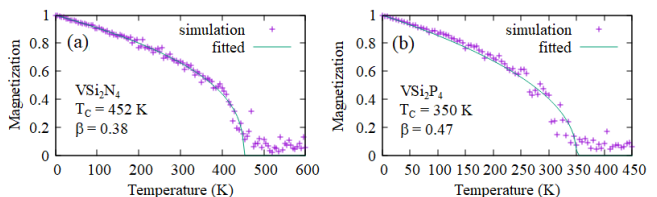


FIG. 3. Monte Carlo calculations of the normalized magnetization as a function of temperature for (a) VSi_2N_4 and (b) VSi_2P_4 . The solid lines show the best fits to the analytical expression given by Eq. (2).

tremely weak in-plane anisotropy, they satisfy the necessary conditions for exhibiting a dissipationless spin superfluid mode.⁴⁷

The normalized magnetizations, determined from Monte Carlo calculations, are plotted as a function of temperature for VSi_2N_4 and VSi_2P_4 in Fig. 3. The solid lines show the best fits to the analytic expression,

$$m(T) = (1 - T/T_C)^\beta. \quad (2)$$

The fitted values of T_C and β are shown on the plots. At the PBE+U level of theory, both monolayer VSi_2P_4 and VSi_2N_4 have Curie temperatures above room temperature, 350 K and 452 K, respectively. The effect of the increasing levels of theory, PBE, PBE+U, and HSE06, is to successively increase the bandgap between the two spin-polarized d_{z^2} bands, so that at the HSE06 level, the two bands are completely gapped which maximizes the spin polarization, magnetic moment, and the exchange constant. The predicted T_C increases with the increasing gap, giving a maximum value of 506 K for VSi_2N_4 using the exchange constant determined from the HSE06 calculation. Since VSi_2N_4 has the same structure, surface chemistry, and formation energy²⁴ as the experimentally characterized MoSi_2N_4 , we expect VSi_2N_4 to also be an air/water-stable material with $T_c > 100^\circ\text{C}$, which is a criterion for operation in a modern integrated circuit environment.

For context, we compare to several other 2D materials with similar predicted Curie or Néel temperatures. The calculated Curie-temperatures for monolayers of the

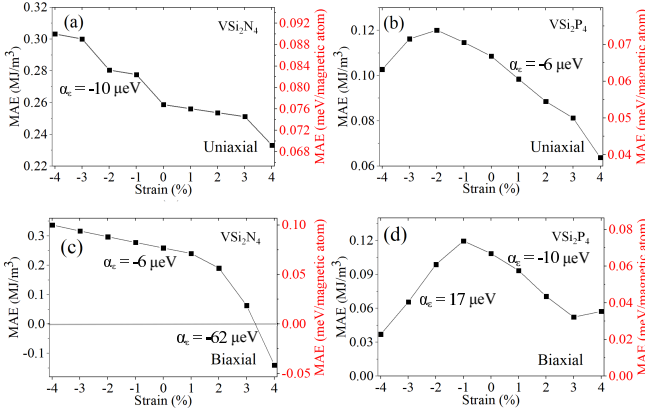


FIG. 4. MAE as a function of uniaxial and biaxial strain calculated with PBE(SOC)+U. MAE versus uniaxial strain: (a) VSi_2N_4 and (b) VSi_2P_4 . MAE versus biaxial strain: (c) VSi_2N_4 and (d) VSi_2P_4 . Values are shown for the strain coefficients for different regions discussed in the text. The orientation of the magnetization of VSi_2N_4 rotates from in-plane to out-of-plane with 3.3% biaxial strain.

transition metal dichalcogenides (TMDs) VS_2 , VSe_2 , and VTe_2 are 292 K, 472 K, and 553 K, respectively.⁴⁸ The predicted monolayer Curie temperatures for the ternary 2D materials CrSeCl , VSeTe , and CrSeI are 320 K, 350 K, and 360 K, respectively.^{16,46,49} Monolayers of ferromagnetic semiconductors TcSiTe_3 have a predicted Curie temperature of 538 K.⁵⁰ We note that Tc is radioactive, so that Tc compounds are unlikely to see magnetic applications. Monolayers of RuI_3 , MnN , Co_2S_2 , and 3R-MoN_2 have Curie temperatures of 360 K, 368 K, 404 K, and 420 K, respectively.^{51–54} We note that synthesis of layered 3R-MoN_2 requires high pressure,⁵⁵ which is not amenable to thin film growth techniques, and the proposed graphitization synthesis route to achieve MnN monolayers⁵⁶ has not yet been demonstrated. Within the list above, VSi_2N_4 stands out for its combination of air stability and relatively high Curie temperature.

The equilibrium values of the MAE are listed in Table I. The equilibrium values of VSi_2N_4 and VSi_2P_4 range from 0.11 to 0.25 meV / magnetic atom. For comparison, monolayers of CrCl_3 , CrBr_3 , and CrI_3 have equilibrium MAEs of 0.02 meV, 0.16 meV, and 0.8 meV, respectively.⁵⁷ Two-dimensional FeCl_2 , NiI_2 , Fe_3P , and Fe_3GeTe_2 have equilibrium MAE values of 0.07 meV, 0.11 meV, 0.72 meV, and 1 meV, respectively in their monolayer limit.^{58–61} In general, the MAE values of VSi_2N_4 , and VSi_2P_4 are on the lower end of values for other 2D magnetic materials.

The calculated values of the MAE of VSi_2N_4 and VSi_2P_4 as a function of uniaxial strain and biaxial strain are shown in Fig. 4. We quantify the sensitivity by defining a strain coefficient as $\alpha_\epsilon = dE_{\text{MAE}}/d\epsilon$. For small strain of both types in both materials, the values for α_ϵ are well below the value of $32 \mu\text{eV}/\% \text{strain}$ recently calculated for a 1.1 nm slab of CrSb .⁶² For compressive

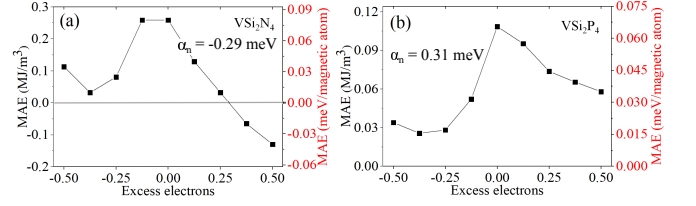


FIG. 5. MAE as a function of band filling calculated with PBE(SOC)+U. MAE as a function of excess electrons per unit cell for (a) VSi_2N_4 and (b) VSi_2P_4 . Values are shown for the filling coefficients discussed in the text. The orientation of the magnetization of VSi_2N_4 rotates from in-plane to out-of-plane with electron doping of $2.0 \times 10^{14} \text{ cm}^{-2}$.

uniaxial and biaxial strain in VSi_2N_4 , $\alpha_\epsilon = -10$ and $-6 \mu\text{eV}/\% \text{strain}$, respectively. For VSi_2P_4 , $\alpha_\epsilon = -6 \mu\text{eV}/\% \text{strain}$ for uniaxial tensile strain, $-10 \mu\text{eV}/\% \text{strain}$ for biaxial tensile strain, and $17 \mu\text{eV}/\% \text{strain}$ for biaxial compressive strain. For large (3-4%) biaxial strain in VSi_2N_4 , the magnitude of the sensitivity increases. At a strain of 3.3%, the MAE changes sign, and the spins rotate from in-plane to out-of-plane. This magnitude of strain should be experimentally accessible, since 2D materials can sustain large strain.⁶³

The effects of band filling on the MAE are shown in Fig. 5. The MAE is reduced in VSi_2N_4 and VSi_2P_4 for both electron and hole doping. To quantify the sensitivity of the MAE to charge filling we define the parameter⁶² $\alpha_n = dE_{\text{MAE}}/dn$ evaluated at zero filling. For electron filling in VSi_2N_4 , $\alpha_n = -0.29 \text{ meV}$, and for hole filling in VSi_2P_4 , $\alpha_n = 0.31 \text{ meV}$. What is most interesting is that the sign of the MAE can be reversed in VSi_2N_4 at an electron filling of 0.28 electrons per unit cell corresponding to a sheet carrier concentration of $n_s = 2.0 \times 10^{14} \text{ cm}^{-2}$. At this doping density, the orientation of the magnetization of VSi_2N_4 rotates from in-plane to out-of-plane. These densities are high, however since the thickness of the monolayer is under 1 nm, such densities could be experimentally accessible using electrolytic gating.

In conclusion, NbSi_2N_4 , VSi_2N_4 , and VSi_2P_4 are easy-plane, semiconducting FMs with negligible in-plane anisotropy. Exchange constants extracted from PBE+U DFT used in MC calculations predict Curie temperatures for monolayer VSi_2P_4 and VSi_2N_4 of 350 K and 452 K, respectively. The effect of the increasing levels of theory, PBE, PBE+U, and HSE06, is to successively increase the energy gap between the two spin-polarized d_{z^2} bands, so that at the HSE06 level, the two bands are completely gapped which maximizes the spin polarization, magnetic moment, and the exchange constant. The predicted T_C increases with the increasing gap, giving a maximum value of 506 K for VSi_2N_4 using the exchange constant determined from the HSE06 calculation. Since VSi_2N_4 has the same structure, surface chemistry, and formation enthalpy as MoSi_2N_4 , it is expected to also be air and water stable. The magnetic anisotropy energies of VSi_2N_4 and VSi_2P_4 , determined by the difference in the

total energies resulting from out-of-plane versus in-plane alignment of the magnetic moments, are small, ranging from 0.11 to 0.25 meV / magnetic atom. Tensile biaxial strain of 3.3% in VSi_2N_4 causes the MAE to change sign such that the magnetic moments rotate from in-plane to out-of-plane. Band filling of 0.28 electrons per unit cell ($2.0 \times 10^{14} \text{ cm}^{-2}$) also causes VSi_2N_4 to switch from in-plane to perpendicular magnetic anisotropy.

Supplementary Material: The supplementary material contains plots of orbital projected band diagrams, comparisons of electronic bandstructures calculated with PBE, PBE+U, and HSE06 functionals, and MC calculations of the normalized magnetization as a function of temperature with exchange constants extracted from PBE DFT. It also contains an extended comparison of Curie temperatures of 2D materials.

Acknowledgement: This work used the Extreme Science and Engineering Discovery Environment (XSEDE),⁶⁴ which is supported by National Science Foundation Grant No. ACI-1548562 and allocation ID TG-DMR130081. MRKA thanks A. Bafekry from University of Guilan, and San-Dong Guo from Xi'an University of Posts and Telecommunications for providing initial crystal structures.

Data Availability Statement: The data that support the findings of this study are available within the article and its supplementary material.

- ¹R. H. Friend and A. D. Yoffe, *Adv. Phys.* **36**, 1 (1987).
- ²R. A. Klemm, *Layered Superconductors*, Vol. 1 (Oxford University Press, New York, 2012).
- ³L. J. de Jongh, ed., *Magnetic Properties of Layered Transition Metal Compounds*, Physics and Chemistry of Materials with Low-Dimensional Structures, Vol. 9 (Kluwer Academic Publishers, 1989).
- ⁴B. Radisavljevic, A. Radenovic, J. Brivio, V. Giacometti, and A. Kis, *Nature nanotechnology* **6**, 147 (2011).
- ⁵S. Kang, D. Lee, J. Kim, A. Capasso, H. S. Kang, J.-W. Park, C.-H. Lee, and G.-H. Lee, *2D Materials* **7**, 022003 (2020).
- ⁶Q. H. Wang, K. Kalantar-Zadeh, A. Kis, J. N. Coleman, and M. S. Strano, *Nature nanotechnology* **7**, 699 (2012).
- ⁷G. Fiori, F. Bonaccorso, G. Iannaccone, T. Palacios, D. Neumaier, A. Seabaugh, S. K. Banerjee, and L. Colombo, *Nature Nanotechnology* **9**, 768 (2014).
- ⁸W. Li, X. Qian, and J. Li, *Nature Reviews Materials* , 1 (2021).
- ⁹B. Huang, G. Clark, E. Navarro-Moratalla, D. R. Klein, R. Cheng, K. L. Seyler, D. Zhong, E. Schmidgall, M. A. McGuire, D. H. Cobden, W. Yao, D. Xiao, P. Jarillo-Herrero, and X. Xu, *Nature* **546**, 270 (2017).
- ¹⁰C. Gong, L. Li, Z. Li, H. Ji, A. Stern, Y. Xia, T. Cao, W. Bao, C. Wang, Y. Wang, Z. Q. Qiu, R. J. Cava, S. G. Louie, J. Xia, and X. Zhang, *Nature* **546**, 265 (2017).
- ¹¹Y. Deng, Y. Yu, Y. Song, J. Zhang, N. Z. Wang, Z. Sun, Y. Yi, Y. Z. Wu, S. Wu, J. Zhu, J. Wang, X. H. Chen, and Y. Zhang, *Nature* **563**, 94 (2018).
- ¹²M. Gibertini, M. Koperski, A. F. Morpurgo, and K. S. Novoselov, *Nature Nanotechnology* **14**, 408 (2019).
- ¹³H. Li, S. Ruan, and Y.-J. Zeng, *Advanced Materials* **31**, 1900065 (2019).
- ¹⁴B. L. Chittari, D. Lee, N. Banerjee, A. H. MacDonald, E. Hwang, and J. Jung, *Phys. Rev. B* **101**, 085415 (2020).
- ¹⁵A. Kabiraj, M. Kumar, and S. Mahapatra, *npj Computational Materials* **6**, 35 (2020).
- ¹⁶R. Han, Z. Jiang, and Y. Yan, *The Journal of Physical Chemistry C* **124**, 7956 (2020).
- ¹⁷P. R. Jothi, J. P. Scheifers, Y. Zhang, M. Alghamdi, D. Stekovic, M. E. Itkis, J. Shi, and B. P. T. Fokwa, *Physica Status Solidi (RRL) - Rapid Research Letters* **14**, 1900666 (2020).
- ¹⁸Y. Khan, S. M. Obaidulla, M. R. Habib, A. Gayen, T. Liang, X. Wang, and M. Xu, *Nano Today* **34**, 100902 (2020).
- ¹⁹Y.-L. Hong, Z. Liu, L. Wang, T. Zhou, W. Ma, C. Xu, S. Feng, L. Chen, M.-L. Chen, D.-M. Sun, X.-Q. Chen, H.-M. Cheng, and W. Ren, *Science* **369**, 670 (2020).
- ²⁰N. Gillgren, D. Wickramaratne, Y. Shi, T. Espiritu, J. Yang, J. Hu, J. Wei, X. Liu, Z. Mao, K. Watanabe, T. Taniguchi, M. Bockrath, Y. Barlas, R. K. Lake, and C. N. Lau, *2D Materials* **2**, 011001 (2014).
- ²¹S.-D. Guo, W.-Q. Mu, Y.-T. Zhu, and X.-Q. Chen, *Phys. Chem. Chem. Phys.* **22**, 28359 (2020).
- ²²L. Cao, G. Zhou, Q. Wang, L. K. Ang, and Y. S. Ang, *Applied Physics Letters* **118**, 013106 (2021).
- ²³S. Li, W. Wu, X. Feng, S. Guan, W. Feng, Y. Yao, and S. A. Yang, *Phys. Rev. B* **102**, 235435 (2020).
- ²⁴L. Wang, Y. Shi, M. Liu, A. Zhang, Y.-L. Hong, R. Li, Q. Gao, M. Chen, W. Ren, H.-M. Cheng, Y. Li, and X.-Q. Chen, *Nature Communications* **12**, 2361 (2021).
- ²⁵A. Bafekry, M. Faraji, D. M. Hoat, M. M. Fadlallah, M. Shahrokhi, F. Shojaei, D. Gogova, and M. Ghergherehchi, *arXiv:2009.04267v1* , 1 (2020).
- ²⁶J. Yu, J. Zhou, X. Wan, and Q. Li, *New Journal of Physics* **23**, 033005 (2021).
- ²⁷Q. Wu, L. Cao, Y. S. Ang, and L. K. Ang, *Applied Physics Letters* **118**, 113102 (2021).
- ²⁸H. Zhong, W. Xiong, P. Lv, J. Yu, and S. Yuan, *Phys. Rev. B* **103**, 085124 (2021).
- ²⁹H. Yao, C. Zhang, Q. Wang, J. Li, Y. Yu, F. Xu, B. Wang, and Y. Wei, *Nanomaterials* **11**, 559 (2021).
- ³⁰G. Kresse and J. Hafner, *Phys. Rev. B* **47**, 558 (1993).
- ³¹P. E. Blochl, *Phys. Rev. B* **50**, 17953 (1994).
- ³²P. Perdew, K. Burke, and M. Ernzerhof, *Phys. Rev. Lett.* **77**, 3865 (1996).
- ³³S. L. Dudarev, G. A. Botton, S. Y. Savrasov, C. J. Humphreys, and A. P. Sutton, *Phys. Rev. B* **57**, 1505 (1998).
- ³⁴J. Heyd, G. E. Scuseria, and M. Ernzerhof, *The Journal of Chemical Physics* **118**, 8207 (2003).
- ³⁵A. V. Krukau, O. A. Vydrov, A. F. Izmaylov, and G. E. Scuseria, *The Journal of Chemical Physics* **125**, 224106 (2006).
- ³⁶A. Kinaci, M. Kado, D. Rosenmann, C. Ling, G. Zhu, D. Banerjee, and M. K. Y. Chan, *Applied Physics Letters* **107**, 262108 (2015).
- ³⁷Y. Wang, D. Puggioni, and J. M. Rondinelli, *Phys. Rev. B* **100**, 115149 (2019).
- ³⁸B. Zimmermann, G. Bihlmayer, M. Böttcher, M. Bouhassoune, S. Lounis, J. Sinova, S. Heinze, S. Blügel, and B. Dupé, *Phys. Rev. B* **99**, 214426 (2019).
- ³⁹B. Schweglinghaus, B. Zimmermann, M. Heide, G. Bihlmayer, and S. Blügel, *Phys. Rev. B* **94**, 024403 (2016).
- ⁴⁰M. Toyoda, K. Yamauchi, and T. Oguchi, *Phys. Rev. B* **87**, 224430 (2013).
- ⁴¹H. J. Xiang, E. J. Kan, S.-H. Wei, M.-H. Whangbo, and X. G. Gong, *Phys. Rev. B* **84**, 224429 (2011).
- ⁴²M. R. K. Akanda, I. J. Park, and R. K. Lake, *Phys. Rev. B* **102**, 224414 (2020).
- ⁴³VAMPIRE software package version 5.0 available from <https://vampire.york.ac.uk>.
- ⁴⁴R. F. L. Evans, W. J. Fan, P. Chureemart, T. A. Ostler, M. O. A. Ellis, and R. W. Chantrell, *J. Phys.: Condens. Matter* **26**, 103202 (2014).
- ⁴⁵F. Subhan and J. Hong, *Journal of Physics: Condensed Matter* **32**, 245803 (2020).
- ⁴⁶H. Wang, J. Qi, and X. Qian, *Applied Physics Letters* **117**, 083102 (2020).
- ⁴⁷S. Takei and Y. Tserkovnyak, *Phys. Rev. Lett.* **112**, 227201 (2014).
- ⁴⁸H.-R. Fuh, C.-R. Chang, Y.-K. Wang, R. F. L. Evans, R. W.

- Chantrell, and H.-T. Jeng, *Scientific Reports* **6**, 32625 (2016).
- ⁴⁹Z. Guan and S. Ni, *Nanoscale* **12**, 22735 (2020).
- ⁵⁰J.-Y. You, Z. Zhang, X.-J. Dong, B. Gu, and G. Su, *Phys. Rev. Research* **2**, 013002 (2020).
- ⁵¹Y. Zhang, J. Pang, M. Zhang, X. Gu, and L. Huang, *Scientific Reports* **7**, 15993 (2017).
- ⁵²C. Huang, J. Zhou, H. Wu, K. Deng, P. Jena, and E. Kan, *Phys. Rev. B* **95**, 045113 (2017).
- ⁵³F. Wu, C. Huang, H. Wu, C. Lee, K. Deng, E. Kan, and P. Jena, *Nano Letters* **15**, 8277 (2015), pMID: 26575002.
- ⁵⁴Z. Xu and H. Zhu, *The Journal of Physical Chemistry C* **122**, 14918 (2018).
- ⁵⁵S. Wang, H. Ge, S. Sun, J. Zhang, F. Liu, X. Wen, X. Yu, L. Wang, Y. Zhang, H. Xu, J. C. Neufeind, Z. Qin, C. Chen, C. Jin, Y. Li, D. He, and Y. Zhao, *Journal of the American Chemical Society* **137**, 4815 (2015), pMID: 25799018.
- ⁵⁶P. B. Sorokin, A. G. Kvashnin, Z. Zhu, and D. Tománek, *Nano Letters* **14**, 7126 (2014), pMID: 25384500.
- ⁵⁷L. Webster and J.-A. Yan, *Phys. Rev. B* **98**, 144411 (2018).
- ⁵⁸H. L. Zhuang, P. R. C. Kent, and R. G. Hennig, *Phys. Rev. B* **93**, 134407 (2016).
- ⁵⁹E. Torun, H. Sahin, C. Bacaksiz, R. T. Senger, and F. M. Peeters, *Phys. Rev. B* **92**, 104407 (2015).
- ⁶⁰S. Zheng, C. Huang, T. Yu, M. Xu, S. Zhang, H. Xu, Y. Liu, E. Kan, Y. Wang, and G. Yang, *The Journal of Physical Chemistry Letters* **10**, 2733 (2019).
- ⁶¹H. Han, H. Zheng, Q. Wang, and Y. Yan, *Phys. Chem. Chem. Phys.* **22**, 26917 (2020).
- ⁶²I. J. Park, S. Kwon, and R. K. Lake, *Phys. Rev. B* **102**, 224426 (2020).
- ⁶³X. Peng, Q. Wei, and A. Copple, *Phys. Rev. B* **90**, 085402 (2014).
- ⁶⁴J. Towns, T. Cockerill, M. Dahan, I. Foster, K. Gaither, A. Grimshaw, V. Hazlewood, S. Lathrop, D. Lifka, G. D. Peterson, *et al.*, *Computing in Science & Engineering* **16**, 62 (2014).

Magnetic Properties of NbSi_2N_4 , VSi_2N_4 , and VSi_2P_4 Monolayers: Supplementary Information

Md. Rakibul Karim Akanda

*Laboratory for Terahertz and Terascale Electronics (LATTE),
Department of Electrical and Computer Engineering,
University of California, Riverside, CA 92521, USA*

Roger K. Lake

*Laboratory for Terahertz and Terascale Electronics (LATTE),
Department of Electrical and Computer Engineering,
University of California, Riverside, CA 92521, USA*

(Dated: August 3, 2021)

Fig. S1 shows the orbital resolved band structure of VSi_2N_4 . Fig. S2 shows the d-orbital resolved band structures of VSi_2N_4 and VSi_2P_4 . Spin resolved PBE, PBE+U, and HSE06 band structures are shown in Fig. S3. Monte Carlo calculations using exchange constants extracted from PBE DFT are shown in Fig. S4.

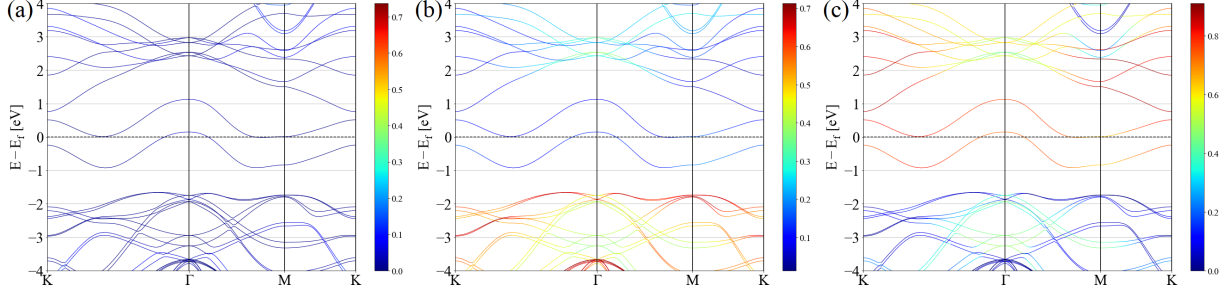


FIG. S1. Orbital resolved PBE band structure of VSi_2N_4 at equilibrium: (a) s-orbital contribution, (b) p-orbital contribution, and (c) d-orbital contribution. The weight is given by the color bars at right. The two isolated, narrow bands near the Fermi level are d-orbital bands centered on the transition metal atoms vanadium (V). The higher valence bands are primarily p-orbital bands which come from the N atoms. The lower conduction bands are primarily d-orbital bands.

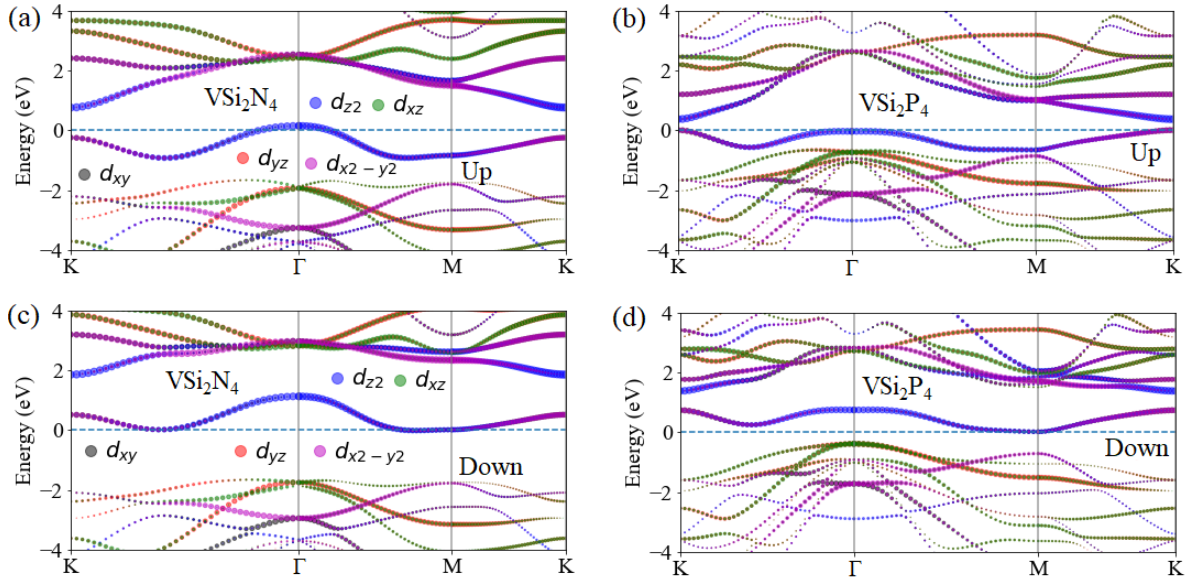


FIG. S2. d-orbital resolved PBE band structure of VSi_2N_4 : (a) spin up bands, (c) spin down bands. d-orbital resolved band structure of VSi_2P_4 : (b) spin up bands, (d) spin down bands.

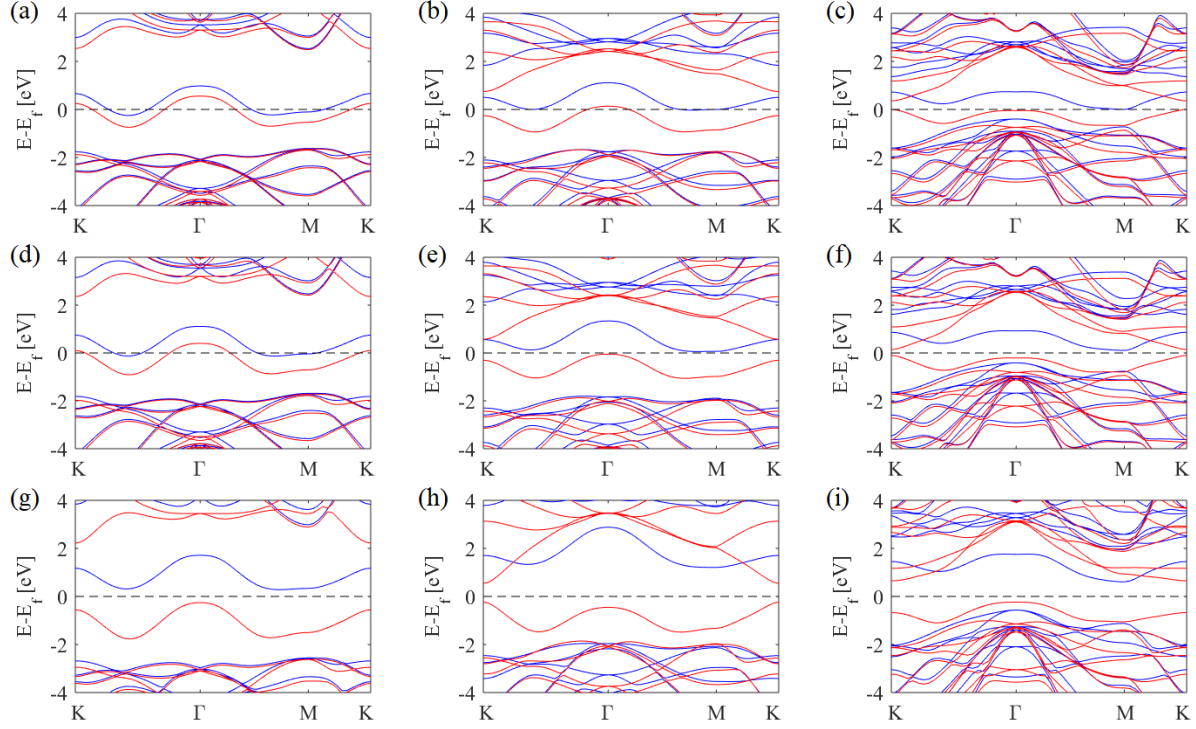


FIG. S3. Spin resolved PBE band structure: (a) NbSi_2N_4 , (b) VSi_2N_4 , and (c) VSi_2P_4 . Spin resolved PBE+U band structure: (d) NbSi_2N_4 , (e) VSi_2N_4 , and (f) VSi_2P_4 . Spin resolved HSE06 band structure: (g) NbSi_2N_4 , (h) VSi_2N_4 , and (i) VSi_2P_4 .

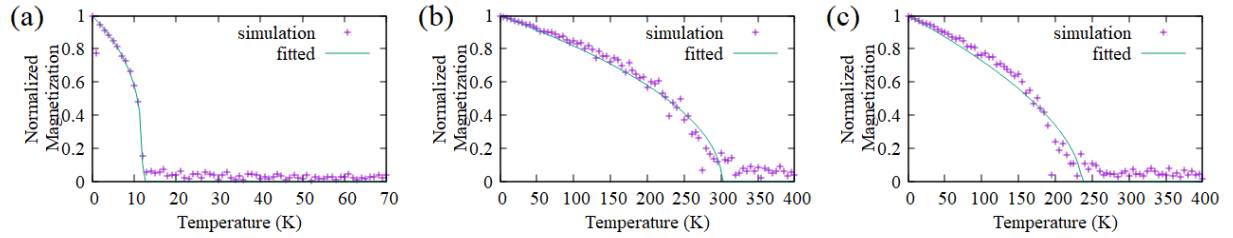


FIG. S4. MC calculations of the normalized magnetization as a function of temperature with exchange constants extracted from PBE DFT for (a) NbSi_2N_4 , (b) VSi_2N_4 , and (c) VSi_2P_4 . Curie temperatures are calculated from Monte Carlo simulation using the VAMPIRE software.